

Ctrl123: Consistent Novel View Synthesis via Closed-Loop Transcription

Hongxiang Zhao^{*1} Xili Dai^{*23} Jianan Wang³ Shengbang Tong⁴ Jingyuan Zhang⁵ Weida Wang⁵
Lei Zhang³ Yi Ma⁶



Figure 1. Ctrl123 generates more pose and appearance consistent novel views from a single image of an arbitrary object.

Abstract

Large image diffusion models have demonstrated zero-shot capability in novel view synthesis (NVS). However, existing diffusion-based NVS methods struggle to generate novel views that are accurately consistent with the corresponding ground truth poses and appearances, even on the training set. This consequently limits the performance of downstream tasks, such as image-to-multiview generation and 3D reconstruction. We realize that such inconsistency is largely due to the fact that it is difficult to enforce accurate pose and appearance alignment directly in the diffusion training, as mostly done by existing methods such as Zero123. To remedy this problem, we propose Ctrl123, a *closed-loop* transcription-based NVS diffusion method that enforces alignment between the generated view and ground truth in a pose-sensitive feature space. Our extensive experiments demonstrate the effectiveness of Ctrl123 on the tasks of NVS and 3D reconstruction, achieving significant improvements in both multiview-

consistency and pose-consistency over existing methods.

1. Introduction

Recent advancements in novel view synthesis (NVS) from a single image have generated significant enthusiasm within the 3D community (Poole et al., 2022; Wang et al., 2023b). NVS is one of the fundamental tasks for any 3D content generation system. It is important for generating a full 3D model from a single image captured by users or generated by text-to-image models. More recently, Zero123 (Liu et al., 2023a) enhances the generalization capability by leveraging powerful pre-trained image generation models such as Stable Diffusion (SD) (Rombach et al., 2022). It fine-tunes Stable Diffusion on image renderings derived from a diverse 3D dataset (Deitke et al., 2023b) to learn to generate a new view conditioned on the reference view and a relative camera transformation. The zero-shot and open-world capabilities of Zero123 represent a significant advancement in the field of NVS. Following the pioneering work of Zero123, subsequent studies (Shi et al., 2023a; Song et al., 2023; Liu et al., 2023b; Shi et al., 2023b) further advanced the overall NVS performance. Zero123-XL (Deitke et al., 2023a) focuses on data quantity, scaling the training data to up to 10 times more; Zero123++ (Shi et al., 2023a) restricts novel view generation from arbitrary view to 6 predetermined views, which significantly reduces the complexity of the setting of the task.

¹Beijing University of Posts and Telecommunications ²Hong Kong University of Science and Technology (Guangzhou) ³International Digital Economy Academy (IDEA) ⁴New York University ⁵Tsinghua-Berkeley Shenzhen Institute (TBSI) ⁶University of California, Berkeley. * Equal Contribution

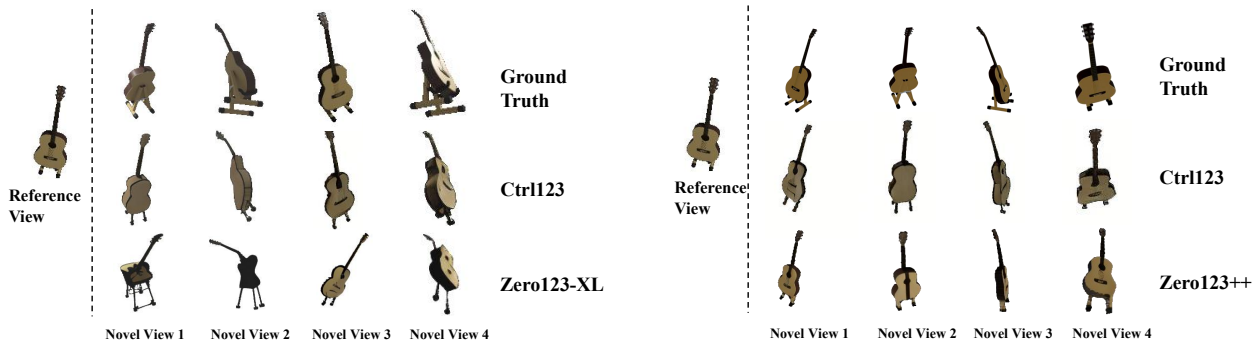


Figure 2. A qualitative comparison of the generated novel views and their corresponding ground truth for an object from the **training set**. Both Zero123-XL and Zero123++ fail to generate results highly consistent with the ground truth in terms of pose and appearance, while Ctrl123 can significantly improve consistency in the generated new views.

Nevertheless, there still exists a fundamental problem in the current NVS models - it is difficult to ensure the generated views to be “**consistent**” with the desired poses and appearances (the ground truth), even on the training images, as demonstrated in Figure 2. Both Zero123-XL and Zero123++ fail to generate novel views with 1) accurate poses closely aligned with the ground truth and 2) high-quality image details, which indicate that this inconsistency problem cannot be resolved by simply scaling up the training dataset or simplifying the task setting.

The inconsistency problem is rooted in the training strategy of diffusion models which separately trains the denoiser at different noise levels. More specifically, in each training step of diffusion models, a random timestep $t \in [0, T]$ is sampled with a pre-defined noising schedule $\bar{\alpha}_t \in (0, 1)$ to corrupt a clean image \mathbf{x} to a noised image \mathbf{x}_t according to $\mathbf{x}_t = \sqrt{\bar{\alpha}_t}\mathbf{x} + \sqrt{1 - \bar{\alpha}_t}\epsilon$, where $\epsilon \sim \mathcal{N}(\mathbf{0}, \mathbf{I})$. Then, a U-Net based conditional denoiser $\phi(\mathbf{x}_t, \mathbf{e}; \omega)$ parameterized by ω , takes \mathbf{x}_t and the condition \mathbf{e} as input and predict the added noise $\hat{\epsilon}$. The denoiser is trained based on the score-matching loss $\min_{\omega} \|\phi(\mathbf{x}_t, \mathbf{e}; \omega) - \epsilon\|_2^2$, at each single noise level t , without any constraints on the whole denoising process (from Gaussian noise \mathbf{x}_T to the clean image \mathbf{x}_0). This strategy significantly improves the diversity of the generated images but neglects the consistency required by NVS models. In this work, we explore ways to enforce consistency between the generated views and ground truth to enhance the capability of NVS models.

One straightforward way to enforce sample-wise consistency is to add a loss such as Mean Square Error (MSE) in the *pixel space* between the generated view and ground truth. However, through extensive experiments, a direct loss in pixel space often leads to training collapse due to the nature of Diffusion Models (see Appendix C for more details). Inspired by the recently proposed closed-loop transcription (CTRL) framework (Dai et al., 2022; Ma et al., 2022; Tong et al., 2022), in this work we propose to align poses of the generated view and ground truth in a **latent**

space using patch features which encode pose information. We name our method Ctrl123, a CTRL-based novel view synthesis method that significantly alleviates the problem of pose inconsistency in NVS. Generally speaking, most current single-image NVS methods (Liu et al., 2023a; Shi et al., 2023a; Weng et al., 2023) can be viewed as an open-loop auto-encoder. In this work, we extend the open-loop framework to a closed-loop one by feeding the generated views into the encoder. We then measure the difference in pose between a generated view and its corresponding ground truth in the latent feature space. To quantitatively measure the pose consistency of the generated views, we introduce metrics (Average Angle (AA) and Intersection over Union (IoU)) into NVS to measure fine-grained and coarse levels of pose-consistency. Through extensive experiments, we show that Ctrl123 significantly improves the NVS pose and appearance consistency which further leads to significantly better 3D reconstruction compared to the current SOTA methods.

The main contributions of this paper are:

- To improve pose and appearance consistency in NVS, we introduce Ctrl123, a novel closed-loop transcription-based novel view synthesis diffusion model that uses patch features to measure (and minimize) differences between generated views and the ground truth.
- An in-depth experiment on a sample set of 25 training objects demonstrates that Ctrl123 exhibits significant superiority to Zero123, generating novel views much more consistent with the ground truth. Quantitatively, Ctrl123 improves the quality of generated views by a **7 point** increase in PSNR. Furthermore, Ctrl123 significantly improves the NVS consistency with a **35.1%** increase in AA^{15°} and **42.5%** increase in IoU^{0.7} (see Table 1).
- Encouraged by these findings, we further train Ctrl123 on a large-scale 3D dataset Objaverse (Deitke et al., 2023b) and observe similar improvements. Ctrl123 improves AA and IoU on three evaluation datasets, with

2.5, 4.9 and 5.5 point improvement on AA^{15°} and 14.8, 9.5, 14.1 point improvement on IoU^{0.7}, respectively.

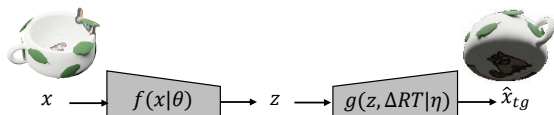
2. Related Work

2.1. Diffusion Models

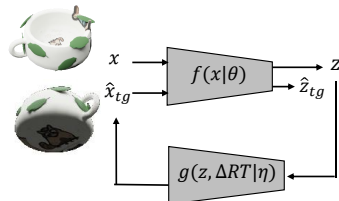
Diffusion models (Ho et al., 2020) demonstrate remarkable capability in image generation. Together with the development of Vision-Language Models such as CLIP (Radford et al., 2021), it accelerates text-to-image (Ramesh et al., 2022; Saharia et al., 2022; Nichol et al., 2021; Rombach et al., 2022) models on large-scale web data (Changpinyo et al., 2021; Schuhmann et al., 2021; 2022). Subsequent works leverage the powerful pre-trained diffusion models for more controllable image generation, conditioning on more fine-grained prompts such as layout, sketch, and human pose (Li et al., 2023b; Zhang et al., 2023). Recent studies have explored distilling knowledge from pre-trained diffusion models for text-to-3D generation through optimizing a differentiable 3D representation with image priors (Poole et al., 2022; Wang et al., 2023a; Chen et al., 2023; Lin et al., 2023; Wang et al., 2023b; Huang et al., 2023). However, this line of work suffers from optimization efficiency, resulting in blurriness and the Janus problem in the generated 3D models. This arises due to the lack of 3D-awareness in pre-trained text-to-image models.

2.2. Novel View Synthesis with Diffusion Models

Novel view synthesis (NVS) requires generating an object’s unobserved geometry and texture, which is a prerequisite capability for 3D generation. Generative models, such as diffusion models (Rombach et al., 2022; Ho et al., 2020) are well-suited for NVS due to their impressive generation capabilities. This is especially advantageous when dealing with sparse input views, to the extreme with a single image. Recently, Zero123 (Liu et al., 2023a) proposes to perform zero-shot open-set NVS by fine-tuning a pre-trained image-to-image diffusion model on multi-view renderings of diverse 3D data (Deitke et al., 2023b). However, this fine-tuning process is computationally expensive and data-demanding. It remains challenging to collect large amounts of high-quality 3D data. As a result, Zero123 often generates inconsistent poses compared to the ground truth. Subsequent efforts (Liu et al., 2023b; Weng et al., 2023; Shi et al., 2023c; Long et al., 2023) aim to resolve view inconsistency by facilitating information propagation across different views which naturally require generating multiple novel views concurrently. Typically, these methods construct training data by fixing an evenly spaced set of camera poses with fixed elevation, and stacking multiple views together to train attention modules that model multi-view dependencies. While these models excel in generating more multi-view consistent novel views, they face challenges in



(a) Existing NVS models (Zero123 and etc.) can be largely viewed as an (open-loop) auto-encoder.



(b) Ctrl123 extends the open-loop NVS models to a closed-loop framework (transcription).

Figure 3. Comparison between the training pipeline of current open-loop NVS models and closed-loop Ctrl123.

generalizing to arbitrary camera poses and remain 3D-data demanding.

3. Method

Our goal is to learn a novel view synthesis (NVS) model that alleviates the “inconsistency” problem by employing the idea of closed-loop transcription (Dai et al., 2022; Ma et al., 2022). To this end, we formulate the current state-of-the-art (SOTA) methods for single-image NVS (Liu et al., 2023a; Shi et al., 2023a; Weng et al., 2023) as an open-loop auto-encoder framework (Section 3.1 and Figure 3(a)). Then, we extend the open-loop to closed-loop to learn the decoder/generator through the closed-loop transcription (CTRL) framework (Section 3.2 and Figure 3(b)). Finally, the choice of training strategy and denoise scheduler are discussed in Section 3.3.

3.1. Current NVS Methods and their Caveats

The Formulation of Current NVS Methods. Given a single RGB image (reference view) of an object, the goal of single image NVS is to synthesize an image of the object from a different camera viewpoint (target view) given the camera transformation. Although various works improve the NVS task in different aspects, we could unify their formulation as an open-loop auto-encoder as follows.

Suppose the random variables \mathbf{X} , ΔRT , and \mathbf{X}_{tg} denote the original image, the camera extrinsic, and the target image, respectively. The dataset \mathcal{D} comprising n triplets represented as $\mathcal{D} = \{(\mathbf{X}^i, \Delta RT_i, \mathbf{X}_{tg}^i)\}_{i=1}^n$, where the given n i.i.d. samples $\mathbf{X}^1, \dots, \mathbf{X}^n \sim \mathbf{X}$, $\Delta RT_1, \dots, \Delta RT_n \sim \Delta RT$, and $\mathbf{X}_{tg}^1, \dots, \mathbf{X}_{tg}^n \sim \mathbf{X}_{tg}$. Specifically, $\Delta RT_i = (\mathbf{R}_i, \mathbf{T}_i)$, where $\mathbf{R}_i \in \mathbb{R}^{3 \times 3}$ and $\mathbf{T}_i \in \mathbb{R}^3$ respectively represent the relative camera rotation and translation. The current single image NVS methods aim to learn a model h that synthesizes new image $\hat{\mathbf{X}}_{tg}$ from the

original image \mathbf{X} under the camera transformation $\Delta\mathbf{RT}$, i.e.,

$$\hat{\mathbf{X}}_{tg} = h(\mathbf{X}, \Delta\mathbf{RT}), \quad (1)$$

where $\hat{\mathbf{X}}_{tg}$ is the synthesized target view. The goal is for $\hat{\mathbf{x}}_{tg}$ to be perceptually similar to the true target view \mathbf{X}_{tg} .

The model h in these methods (Liu et al., 2023a; Shi et al., 2023a; Liu et al., 2023b) is composited by an encoder $f : \mathbf{X} \mapsto \mathbf{Z}$, parameterized by θ , and a decoder $g : (\mathbf{Z}, \Delta\mathbf{RT}) \mapsto \hat{\mathbf{X}}_{tg}$, parameterized by η , i.e., $h(\mathbf{X}, \Delta\mathbf{RT}) = g(f(\mathbf{X}), \Delta\mathbf{RT})$. Specifically, the encoder f is commonly chosen to be the ViT (Dosovitskiy et al., 2020) model of a pre-trained CLIP (Radford et al., 2021) and kept frozen during the NVS training. Let $\mathbf{Z} = f(\mathbf{X}, \theta) \in \mathbb{R}^d$, where \mathbf{Z} is the class feature (cls token) of ViT.

The decoder g is commonly implemented as a process of multi-step conditional denoising (Liu et al., 2023a). First, the process is conditioned on a transformation $e = \psi(\mathbf{Z}, \Delta\mathbf{RT})$ of the feature \mathbf{Z} and delta pose $\Delta\mathbf{RT}$, where ψ is a multi-layer perception. Then, for step $t \in \{0, \dots, T\}$, the noise $\hat{\epsilon}$ is predicted, using an U-net ϕ , based on the predicted target view at time step t , and the condition e , i.e., $\hat{\epsilon} = \phi(\hat{\mathbf{X}}_t, e)$ ¹.

The multi-step denoising process is performed through a denoiser $\mathcal{S}(\cdot)$, based on denoising diffusion implicit models (DDIM) (Song et al., 2020). The predicted target view at time step $t-1$ is generated by the denoiser and the predicted target view and noise, i.e., $\hat{\mathbf{X}}_{t-1} = \mathcal{S}(\hat{\mathbf{X}}_t, \hat{\epsilon})$ ². As for the initial step $t = T$, the target view $\hat{\mathbf{X}}_T$ is randomly sampled from isotropic Gaussian.

We denote random variable $\hat{\mathbf{X}}_{tg} \doteq g(\mathbf{Z}, \Delta\mathbf{RT})$ as the decoded image from Gaussian noise $\hat{\mathbf{X}}_T$ through T denoising steps according to \mathcal{S} conditioned on \mathbf{Z} and $\Delta\mathbf{RT}$. Current single-image NVS methods can be summarized as the following open-loop framework,

$$\mathbf{X} \xrightarrow{f(\mathbf{X}, \theta)} \mathbf{Z} \xrightarrow{g(\mathbf{Z}, \Delta\mathbf{RT}, \eta)} \hat{\mathbf{X}}_{tg}. \quad (2)$$

Such diffusion-based NVS methods typically adopt a standard diffusion training strategy by supervising single-step denoising results with a score-matching loss, i.e.,

$$\min_{\phi, \psi} \mathbb{E} \|\phi(\mathbf{X}_t, \psi(\mathbf{Z}, \Delta\mathbf{RT})) - \epsilon\|_2^2, \quad (3)$$

where the expectation is taken over the encoded feature \mathbf{Z} , timestep t , and randomly sampled Gaussian noise ϵ .

¹For simplicity, we use $\hat{\mathbf{X}}_t$ instead of $\hat{\mathbf{X}}_{tg,t}$ which is the target view with t steps noise

² $\mathcal{S}(\hat{\mathbf{X}}_t, \hat{\epsilon}) = \frac{1}{\sqrt{\bar{\alpha}_t}} (\hat{\mathbf{X}}_t - \frac{1-\bar{\alpha}_t}{\sqrt{1-\bar{\alpha}_t}} \hat{\epsilon})$ where $\bar{\alpha}_t = \prod_{i=1}^t \alpha_i$ and $\alpha_t = 1 - \beta_t$, β_t is a pre-defined variance of t -th step.

The Caveats of Current NVS Methods. While the showcased results in most single-image NVS works appear impressive, we make a critical observation previously overlooked: the generated novel views often lack consistency with the ground truth, even when evaluated on the training data, as exemplified in Figure 2. This inconsistency problem is rooted in the training strategy of diffusion models which separately trains the denoiser at different noise levels using solely score matching loss without any constraints on the whole denoising process (from Gaussian noise \mathbf{X}_T to the clean image \mathbf{X}_0). This strategy significantly improves the diversity of the generated images but neglects the consistency required in NVS models. In this work, we explore ways to enforce consistency between the generated views and ground truth to enhance the capability of NVS models.

3.2. Ctrl123: Consistency via a Closed-Loop Framework

A straightforward method to enforce sample-wise consistency is to add a loss such as Mean Square Error (MSE) in the *pixel space* between the generated view $\hat{\mathbf{X}}_{tg}$ and ground truth \mathbf{X}_{tg} . However, through extensive experiments, a direct loss in pixel space often suffers training difficulties leading to training collapse (See Appendix C for more details).

The recently proposed *closed-loop transcription* (CTRL) framework (Dai et al., 2022) is naturally suited to solve this problem. The difference between \mathbf{X} and $\hat{\mathbf{X}}$ can be measured through the distance between their corresponding features \mathbf{Z} and $\hat{\mathbf{Z}} = f(\hat{\mathbf{X}}, \theta)$ mapped through the same encoder, i.e.,

$$\mathbf{X} \xrightarrow{f(\mathbf{X}, \theta)} \mathbf{Z} \xrightarrow{g(\mathbf{Z}, \eta)} \hat{\mathbf{X}} \xrightarrow{f(\hat{\mathbf{X}}, \theta)} \hat{\mathbf{Z}}. \quad (4)$$

Inspired by CTRL, we apply this idea to the current NVS model that measures the difference between \mathbf{X}_{tg} and the generated $\hat{\mathbf{X}}_{tg}$ in the latent space. In other words, we apply it to diagram 2 to get the following new diagram:

$$\mathbf{X} \xrightarrow{f(\mathbf{X}, \theta)} \mathbf{Z} \xrightarrow{g(\mathbf{Z}, \Delta\mathbf{RT}, \eta)} \hat{\mathbf{X}}_{tg} \xrightarrow{f(\hat{\mathbf{X}}_{tg}, \theta)} \hat{\mathbf{Z}}_{tg}. \quad (5)$$

Different from the direct CTRL formulation equation 4, we can not directly calculate the loss between \mathbf{Z} and $\hat{\mathbf{Z}}_{tg}$ since they are the features of different views. Hence, we add the feature \mathbf{Z}_{tg} of the ground truth target view \mathbf{X}_{tg} as the following,

$$\begin{aligned} \mathbf{X} \xrightarrow{f(\mathbf{X}, \theta)} \mathbf{Z} \xrightarrow{g(\mathbf{Z}, \Delta\mathbf{RT}, \eta)} \hat{\mathbf{X}}_{tg} \xrightarrow{f(\hat{\mathbf{X}}_{tg}, \theta)} \hat{\mathbf{Z}}_{tg}, \\ \mathbf{X}_{tg} \xrightarrow{f(\mathbf{X}_{tg}, \theta)} \mathbf{Z}_{tg}. \end{aligned} \quad (6)$$

Now we can measure the \mathbf{Z}_{tg} and $\hat{\mathbf{Z}}_{tg}$ through Mean Squared Error $\min_g \|\mathbf{Z}_{tg} - \hat{\mathbf{Z}}_{tg}\|_2^2$.

Building upon the previously established definition of \mathbf{Z} , we identify it as the class feature within the outputs of the Vision Transformer (ViT) model. Revisiting the ViT model, its outputs are bifurcated into class features and patch features. The class features capture high-level information, whereas the patch features are indicative of low-level information. Our methodology prioritizes the analysis of patch features due to their richer informational content, which significantly aligns with ground truth data and enhances consistency. This preference is empirically validated in our ablation study, which demonstrates superior performance of patch features over class features (refer to Appendix C for detailed results).

To accommodate this distinction, we introduce a revised notation for the encoder outputs, denoted as $[\mathbf{Z}_c, \mathbf{Z}_p] = f(\mathbf{X}, \theta)$ and $[\mathbf{Z}_{tg,c}, \mathbf{Z}_{tg,p}] = f(\mathbf{X}_{tg}, \theta)$, where \mathbf{Z}_c and $\mathbf{Z}_{tg,c}$ represent the high-level class features, and \mathbf{Z}_p and $\mathbf{Z}_{tg,p}$ correspond to the low-level patch features. Re-writing the diagram 6 with the re-defined notation as the following,

$$\mathbf{X} \xrightarrow{f(\mathbf{X}, \theta)} \mathbf{Z}_c \xrightarrow{g(\mathbf{Z}_c, \Delta RT, \eta)} \hat{\mathbf{X}}_{tg} \xrightarrow{f(\mathbf{X}, \theta)} \hat{\mathbf{Z}}_{tg,p} \quad (7)$$

$$\mathbf{X}_{tg} \xrightarrow{f(\mathbf{X}, \theta)} \mathbf{Z}_{tg,p}$$

where \mathbf{Z}_c is the class feature of reference views \mathbf{X} and $\mathbf{Z}_{tg,p}$ is the patch feature of target view \mathbf{X}_{tg} , and we can measure the $\mathbf{Z}_{tg,p}$ and $\hat{\mathbf{Z}}_{tg,p}$ through Mean Squared Error,

$$\min_g \|\mathbf{Z}_{tg,p} - \hat{\mathbf{Z}}_{tg,p}\|_2^2. \quad (8)$$

3.3. Denoise Scheduler & Alternative Training Strategy

Denoise Scheduler. It is slow to generate a sample from DDPM by following the Markov chain of the reverse diffusion process, as T can be as many as a few thousand steps. One simple way to accelerate the process is to run a strided sampling schedule with every $\lceil T/S \rceil$ steps to reduce the process from T to S steps. The new sampling schedule for generation is $\{\tau_1, \dots, \tau_S\}$ where $\tau_1 < \tau_2 < \dots < \tau_S \in [1, T]$ and $S < T$. During generation, we only sample a subset of S diffusion steps and the inference process becomes:

$$\hat{\mathbf{X}}_{\tau_{s-1}} = \frac{1}{\sqrt{\bar{\alpha}_t}} \left(\mathbf{X}_{\tau_s} - \frac{1 - \alpha_{\tau_s}}{\sqrt{1 - \bar{\alpha}_{\tau_s}}} \hat{\epsilon}_{\tau_s} \right), \quad (9)$$

where $s \in \{1, \dots, S\}$ and $\bar{\alpha}_t = \prod_{i=1}^t \alpha_i$ and $\alpha_t = 1 - \beta_t$, β_t is a pre-defined variance of t -th step. In this paper, we conduct ablation studies on the choice of S and use $S = 50$ throughout our experiments.

Alternative Training Strategy. Instead of directly applying Equation (8) as a regularization term over the score-matching loss, we propose an alternative training strategy which is ablated in Table 3. We perform fine-tuning on pre-trained Zero123 (Liu et al., 2023a). One round of training

involves 1) m iterations of closed-loop training via CTRL framework as depicted in 7 with supervision loss according to Equation (8). We call this process CL training; 2) n iterations of standard diffusion model fine-tuning with score-matching loss. We call this process SM training for short. Our experiment results show that more rounds of such training could continuously improve NVS performance. Such an alternative training strategy is more efficient and practical as the hyper-parameters of CL training and SM training are vastly different. It is time-consuming and energy-inefficient to grid search a sweet spot of hyper-parameters for both CL and SM training. In section 4.5 we demonstrate the effectiveness of this alternative training strategy.

4. Experiments

We evaluate Ctrl123 on the tasks of single-view NVS and 3D reconstruction. 3D reconstruction is a more challenging task that requires strong multiview consistency. In Section 4.1, we describe our data collating and the implementation details. We introduce the metrics used to measure pose consistency between the generated novel views and the ground truth in Section 4.2, including our proposed metric Angle Accuracy (AA) and Intersection over Union (IoU). We provide in Section 4.3 results on both small-scale and large-scale experiments, trained on a subset of the curated dataset and the full dataset, respectively. Results on 3D reconstruction are provided in Section 4.4. Ablations on the design choices are presented in Section 4.5.

Table 1. Ablation study on the number of rounds for alternative training strategy, measured with 4 metrics: KID(\downarrow), PSNR(\uparrow), AA^{x° (\uparrow), and IoU^{x° (\uparrow).

Method vs. Metrics	Training steps	Image Quality	Alignment (MegaPose/DIS)
Zero123-small	20,000	KID:0.0254 PSNR:19.3839	AA^{15° :22.62% $IoU^{0.7}$:30.93%
Ctrl123-small (1 round)	10,000	KID:0.0087 PSNR:23.6080	AA^{15° :32.02% (+9.40%) $IoU^{0.7}$:55.01% (+24.08%)
Ctrl123-small (2 rounds)	20,000	KID:0.0067 PSNR:26.5348	AA^{15° :57.78% (+35.16%) $IoU^{0.7}$:73.44% (+42.51%)

4.1. Settings

Dataset and Baseline. We use Zero123 (Liu et al., 2023a) as our baseline, and utilize the public 3D dataset - Objaverse (Deitke et al., 2023b) which contains around 800K diverse 3D models created by artists. For training efficiency and quality, we apply the data curation similar to Li et al. (2023a), eliminating 3D assets with sub-optimal geometry, low-quality texture, or small sizes. This curation process results in a refined training dataset with approximately 100K 3D models. All other configurations follow the settings in the literature of baseline (e.g. the number of view sampling, sampling strategy, and camera model, among others).

Table 2. Quantitative comparison of Ctrl123 and Zero123 trained on 100K Objaverse assets, measured with 4 different metrics: PSNR (\uparrow), KID (\downarrow), AA^{x° (\uparrow), and IoU^{x° (\uparrow), and evaluated on 3 datasets: GSO, RTMV, and 25 randomly sampled objects from the training set.

Method	GSO				RTMV				25 Training Objects			
	PSNR	KID	AA^{15°	$IoU^{0.7}$	PSNR	KID	AA^{15°	$IoU^{0.7}$	PSNR	KID	AA^{15°	$IoU^{0.7}$
Zero123	17.2049	0.0055	14.41%	47.32%	8.9123	0.0340	7.04%	2.91%	15.9452	0.0043	14.28%	31.86%
Ctrl123	18.4712	0.0045	16.96%	62.11%	10.8938	0.0294	11.98%	12.41%	18.9398	0.0052	19.79%	45.97%

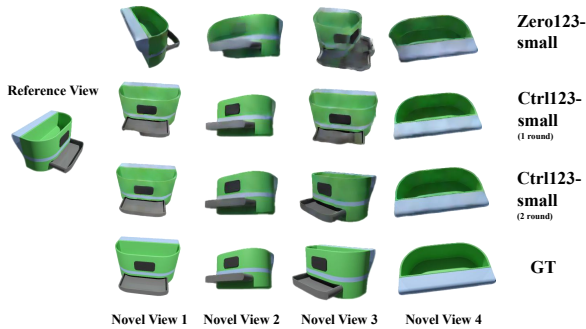


Figure 4. Comparison of the quality and pose consistency between the generated novel views and the corresponding ground truth. While Zero123 generates low-quality pose-inconsistent novel views, Ctrl123 produces significantly more consistent results which continue to improve with more rounds of alternative training. Please refer to Appendix A.1 for more visualization results.

Implementation. We train Ctrl123 on 100K curated Objaverse 3D models for 2 rounds of alternative training. We initialize Ctrl123 with pre-trained weights of Zero123 and train on 8 A100 GPUs. For each alternative training round, we conduct 500 steps of closed-loop (CL) training with a total batch size of 320 and a learning rate of 10^{-4} , followed by 1000 steps of score-matching (SM) training with a total batch size of 1536 and a learning rate of 10^{-5} , each taking around 2 days. We use gradient accumulation to increase the training batch size, 2 for CL training and 1000 for SM training respectively. During model training, we use the Adam optimizer (Kingma & Ba, 2014) with $\beta_1 = 0.9$ and $\beta_2 = 0.99$. In all the experiments, we train our model with the 16-bit floating point (fp16) format for efficiency.

4.2. Angle Accuracy (AA) and Intersection over Union (IoU)

The uniqueness of NVS makes the evaluation a multifaceted problem. We cannot *only* evaluate the model’s performance via traditional image generation benchmarks such as KID, FID, PSNR, and SSIM. As discussed in Sections 1 and 3, it is equally important to evaluate the model’s ability to generate pose “consistent” views. In doing so, we introduce two metrics **Angle Accuracy (AA)** and **Intersection over Union (IoU)** that measure pose consistency on both *fine-grained* and *coarse* level.

Angle Accuracy (AA). AA is first introduced in Zhou et al. (2019). For each camera pose predicted in the generated novel view, we calculate the angle between the ground truth and the predicted pose. We then identify the percentage of predictions where the angle difference falls within a predefined threshold. By altering these thresholds, we can plot *angle accuracy curves*. AA^{x° is defined as the area under the curve between $[0, x^\circ]$ divided by x° . The development of the 6D pose estimation task enables the prediction of 6D pose from a single image with its GT CAD model. In this work, we use MegaPose (Labbé et al., 2023) which is a single image pose estimator, to estimate the camera pose of the generated view.

Intersection over Union (IoU). We also employ a segmentation metric IoU (Garcia-Garcia et al., 2017) that captures more coarse aspect of pose consistency. We use DIS (Qin et al., 2022) to predict the mask of the generated view and the ground truth view to measure the IoU. The calculation of IoU is defined by dividing the overlap between the predicted and ground truth mask by the union of them.

For all experiments in this paper, we report KID(\downarrow), PSNR(\uparrow), AA^{x° (\uparrow) and IoU^{x° (\uparrow) to compare the high-level quality, low-level details, and pose consistency of the generated novel views among all methods. (\uparrow) denotes the higher the better, verse vice for (\downarrow).

4.3. Comparison with SOTA

Improvement with Multi-rounds Optimization. First, we evaluate the performance of multi-rounds training strategy of Ctrl123 on a small dataset. The dataset consists of 25 objects from Objaverse, each with 12 randomly sampled views. We first train a baseline (Zero123-small in Table 1), which is initialized with pre-trained weights of Stable Diffusion, and then fine-tuned on the 25 objects by score matching loss for 20,000 iterations with batch size of 6. We train Ctrl123-small following the alternative training strategy as detailed section 3.3. For fair comparison, it is initialized with the checkpoint of Zero123-small at 10,000 iterations. We train for 500 closed-loop iterations and 4,500 score-matching iterations as one round. Therefore, after two rounds of training, Ctrl123-small will accumulate the same number of training iterations as the baseline (20,000).

As shown in Table 1 and Figure 4, Ctrl123 significantly

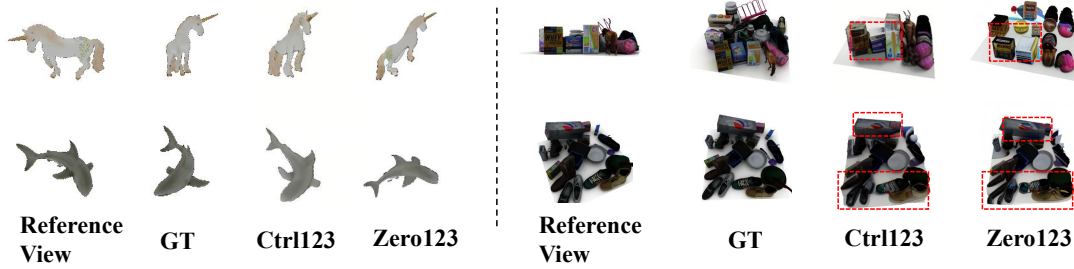


Figure 5. Qualitative comparison of NVS generalization capability on GSO (Left) and RTMV (Right) after training on large-scale dataset (100K). More cases can be found in Appendix A.2.



Figure 6. Qualitative comparison of data fitting capability on 25 training objects after training on large-scale dataset (100K). More cases can be found in Appendix A.2.

improves over Zero123 both qualitatively and quantitatively. Even with fewer training steps, Ctrl123 achieves better KID, PSNR, AA and IoU scores. After 2 rounds of training, the PSNR increases by 7.2 points which is almost $2\times$ better than baseline³. Ctrl123 also generates more pose-consistent views. On the fine-grained level, AA increases from 22.62% to 57.78%; One a more coarse level, IoU increases from 30.94% to 73.44%.

Improvements extend to larger datasets. Following Zero123 (Liu et al., 2023a), we evaluate on GSO (Downs et al., 2022) and RTMV (Tremblay et al., 2022) for NVS quality in Table 2. Each environment evaluates 20 randomly selected objects/scenes rendered for 17 randomly sampled views from the test set. As shown in Table 2, Ctrl123 outperforms Zero123 in all four metrics (PSNR, KID, AA^{x° , and IoU^{x°) and all three evaluation datasets (GSO, RTMV, and 25 training objects). In particular, Ctrl123 obtains much better pose-consistency (see AA^{x° , and IoU^{x°). We visualize the differences in Figure 5 and Figure 6 for qualitative comparison. Ctrl123 generates higher quality and more pose-consistent views comparing to the baseline.

³Based on the definition of PSNR, 3 points equals $1\times$ visual quality improvement (Wang et al., 2004)

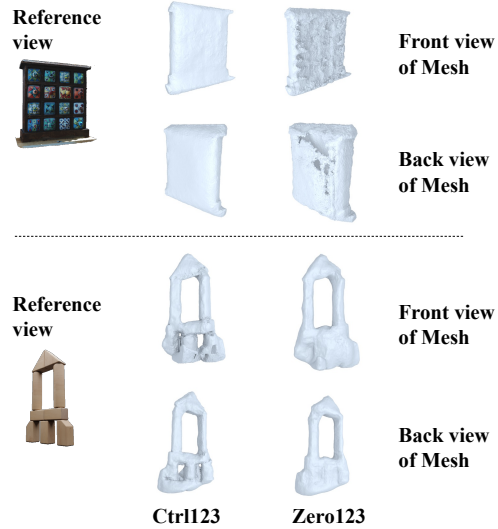


Figure 7. Qualitative comparison of 3D reconstruction from single view images with different methods (Ctrl123 vs Zero123).

4.4. 3D Reconstruction

We also evaluate 3D reconstruction of Ctrl123 on Objaverse instances, as well as randomly selected web images. We use the SDS (Poole et al., 2022) loss implemented by threestudio (Guo et al., 2023) for 3D reconstruction. We then evaluate qualitatively on the exported mesh from reconstructed 3D (refer to Appendix B for implementation details). Figure 7 shows the comparison of the generated 3D mesh. Ctrl123 exhibits better reconstruction quality with smooth surfaces and detailed geometry.

Figure 8 and 9 show the NVS and 3D reconstruction results on both the training set and images in the wild. Ctrl123 performs higher-fidelity and finer detail 3D reconstruction, and multi-view consistent pose consistent novel view synthesis. Figure 7 shows the NVS/3D mesh comparison with other NVS methods. In comparison, Ctrl123 achieves the best reconstruction quality with smooth surfaces and detailed geometry.

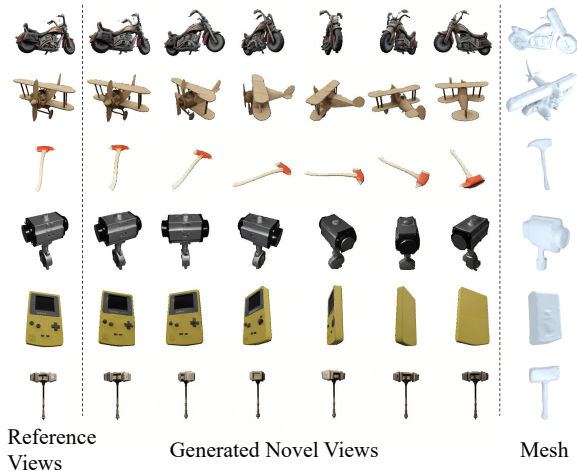


Figure 8. NVS/3D examples using Ctrl123 on images from training set (100K).

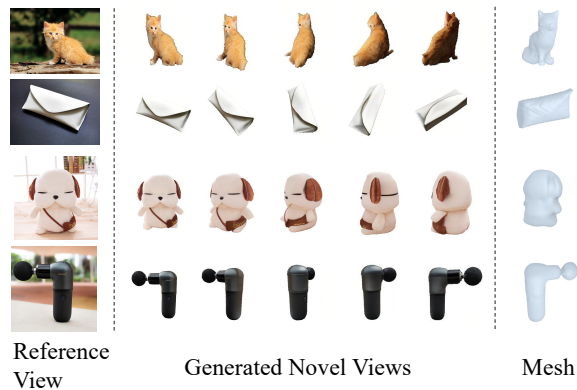


Figure 9. NVS/3D examples using Ctrl123 on images in-the-wild.

4.5. Ablation Study

We conduct ablation studies to verify the importance of multi-step distillation and alternative training strategies (Section 3.3). We sample a subset of Objaverse, 25 objects with 12 randomly sampled views for the ablation studies.

Different Training Strategy. In Section 3.3, the “Simultaneous” implementation of the training strategy involves adding Equation 8 as a regularization term to the score-matching loss of Zero123, with the aim of optimizing both simultaneously. In Table 3, the row “Alternative” is the results of the row “Ctrl123-small(1 round)” in Table 1. We implement “Simultaneous” by changing the loss of the experiment “Ctrl123-small(1 round)” from the alternative version to the simultaneous version. All other settings like learning rate, optimizer etc are the same. The results in Table 3 shows the “Alternative” strategy is better.

Denoise Scheduler. As discussed in Section 3.3, the number of denoising steps used in the function g to generate \hat{X}_{tg} is crucial for balancing the quality of \hat{X}_{tg} against memory consumption. To investigate this, we conducted experiments

Table 3. Ablation study on the optimization strategies.

Strategy	Image Quality	Alignment(MegaPose/DIS)
Simultaneous	KID:0.0218	AA ^{15°} :25.21%
	PSNR:17.9643	IoU ^{0.7} :35.41%
Alternative	KID:0.0087	AA ^{15°} :32.02%
	PSNR:23.6080	IoU ^{0.7} : 55.01%

Table 4. Ablation study on the number of denoise steps for \hat{X}_{tg} generation.

Method vs. Metrics	Image Quality	Alignment(MegaPose/DIS)
Zero123	KID :0.0254 PSNR :19.3839	AA ^{15°} :22.62% IoU ^{0.7} :30.93%
Ctrl123 (1 denoise steps)	KID:0.0194 PSNR :20.1593	AA ^{15°} :23.56% IoU ^{0.7} :32.18%
Ctrl123 (10 denoise steps)	KID:0.0102 PSNR:22.5739	AA ^{15°} :25.71% IoU ^{0.7} :38.97%
Ctrl123 (30 denoise steps)	KID:0.0095 PSNR:23.1165	AA ^{15°} :29.47% IoU ^{0.7} :49.32%
Ctrl123 (50 denoise steps)	KID: 0.0087 PSNR:23.6080	AA ^{15°} :32.02% IoU ^{0.7} : 55.01%

with different numbers of denoising steps (1, 10, 30, 50) to evaluate their impact on image quality and pose alignment. The results, presented in Table 4, indicate that the pose alignment improves as the number of denoising steps increases while image quality improvement stops at the 30 steps. We choose denoise step 50 since the pose alignment is the property that we care the most.

5. Conclusion

In this paper, we introduce Ctrl123, a closed-loop transcription-based NVS method that significantly alleviates the problem of pose and appearance inconsistency between the generated view and ground truth in NVS. To quantitatively measure the performance of consistency improved by Ctrl123, we introduce metrics AA and IoU. Through extensive experiments, we show that the closed-loop Ctrl123 significantly improves pose-consistency (and appearance consistency) for NVS, and leads to significantly better 3D reconstruction compared to the current SOTA methods. Note that in (Ma et al., 2022) the closed-loop framework is proposed as a general framework for ensuring consistency. The work of (Dai et al., 2022) has shown that the closed-loop formulation is also effective in ensuring consistency for image classes, besides poses. Hence we believe such a closed-loop framework is necessary to ensure consistency in content generation for other attributes, such as relative pose between objects, as well as their shapes and textures etc. We will leave such generalization to future investigation.

6. Impact Statement

This paper presents work whose goal is to advance the field of Machine Learning. There are many potential societal consequences of our work. Our work shows the general closed-loop framework may significantly improve the controllability of generative models for generating 2D images and 3D contents with desired precise attributes. Once widely adopted, the framework can significantly improve the quality of generated images, videos, and virtual objects, fundamentally enhance industrial technologies and applications for digital design and augmented reality.

References

- Changpinyo, S., Sharma, P., Ding, N., and Soricut, R. Conceptual 12M: Pushing Web-Scale Image-Text Pre-Training To Recognize Long-Tail Visual Concepts. In *Proceedings of the IEEE/CVF Conference on Computer Vision and Pattern Recognition*, pp. 3558–3568, 2021.
- Chen, R., Chen, Y., Jiao, N., and Jia, K. Fantasia3d: Disentangling geometry and appearance for high-quality text-to-3d content creation. *arXiv preprint arXiv:2303.13873*, 2023.
- Dai, X., Tong, S., Li, M., Wu, Z., Psenka, M., Chan, K. H. R., Zhai, P., Yu, Y., Yuan, X., Shum, H.-Y., et al. Ctrl: Closed-loop transcription to an ldr via minimizing rate reduction. *Entropy*, 24(4):456, 2022.
- Deitke, M., Liu, R., Wallingford, M., Ngo, H., Michel, O., Kusupati, A., Fan, A., Laforte, C., Voleti, V., Gadre, S. Y., et al. Objaverse-xl: A universe of 10m+ 3d objects. *arXiv preprint arXiv:2307.05663*, 2023a.
- Deitke, M., Schwenk, D., Salvador, J., Weihs, L., Michel, O., VanderBilt, E., Schmidt, L., Ehsani, K., Kembhavi, A., and Farhadi, A. Objaverse: A Universe of Annotated 3D Objects. In *Proceedings of the IEEE/CVF Conference on Computer Vision and Pattern Recognition*, pp. 13142–13153, 2023b.
- Dosovitskiy, A., Beyer, L., Kolesnikov, A., Weissenborn, D., Zhai, X., Unterthiner, T., Dehghani, M., Minderer, M., Heigold, G., Gelly, S., et al. An image is worth 16x16 words: Transformers for image recognition at scale. *arXiv preprint arXiv:2010.11929*, 2020.
- Downs, L., Francis, A., Koenig, N., Kinman, B., Hickman, R., Reymann, K., McHugh, T. B., and Vanhoucke, V. Google scanned objects: A high-quality dataset of 3d scanned household items. In *2022 International Conference on Robotics and Automation (ICRA)*, pp. 2553–2560. IEEE, 2022.
- Garcia-Garcia, A., Orts-Escolano, S., Oprea, S., Villena-Martinez, V., and Garcia-Rodriguez, J. A review on deep learning techniques applied to semantic segmentation. *arXiv preprint arXiv:1704.06857*, 2017.
- Guo, Y.-C., Liu, Y.-T., Shao, R., Laforte, C., Voleti, V., Luo, G., Chen, C.-H., Zou, Z.-X., Wang, C., Cao, Y.-P., and Zhang, S.-H. threestudio: A unified framework for 3d content generation. <https://github.com/threestudio-project/threestudio>, 2023.
- Ho, J., Jain, A., and Abbeel, P. Denoising Diffusion Probabilistic Models. *Advances in Neural Information Processing Systems*, 33:6840–6851, 2020.
- Huang, Y., Wang, J., Shi, Y., Qi, X., Zha, Z.-J., and Zhang, L. Dreamtime: An improved optimization strategy for text-to-3d content creation. *arXiv preprint arXiv:2306.12422*, 2023.
- Kingma, D. P. and Ba, J. Adam: A method for stochastic optimization. *CoRR*, abs/1412.6980, 2014. URL <https://doi.org/10.48550/arXiv.1412.6980>.
- Labbé, Y., Manuelli, L., Mousavian, A., Tyree, S., Birchfield, S., Tremblay, J., Carpentier, J., Aubry, M., Fox, D., and Sivic, J. Megapose: 6d pose estimation of novel objects via render & compare. In *Conference on Robot Learning*, pp. 715–725. PMLR, 2023.
- Langley, P. Crafting papers on machine learning. In Langley, P. (ed.), *Proceedings of the 17th International Conference on Machine Learning (ICML 2000)*, pp. 1207–1216, Stanford, CA, 2000. Morgan Kaufmann.
- Li, J., Tan, H., Zhang, K., Xu, Z., Luan, F., Xu, Y., Hong, Y., Sunkavalli, K., Shakhnarovich, G., and Bi, S. Instant3d: Fast text-to-3d with sparse-view generation and large reconstruction model. *arXiv preprint arXiv:2311.06214*, 2023a.
- Li, Y., Liu, H., Wu, Q., Mu, F., Yang, J., Gao, J., Li, C., and Lee, Y. J. GLIGEN: Open-Set Grounded Text-to-Image Generation. In *Proceedings of the IEEE/CVF Conference on Computer Vision and Pattern Recognition*, pp. 22511–22521, 2023b.
- Lin, C.-H., Gao, J., Tang, L., Takikawa, T., Zeng, X., Huang, X., Kreis, K., Fidler, S., Liu, M.-Y., and Lin, T.-Y. Magic3D: High-Resolution Text-to-3D Content Creation. In *Proceedings of the IEEE/CVF Conference on Computer Vision and Pattern Recognition*, pp. 300–309, 2023.
- Liu, R., Wu, R., Van Hoorick, B., Tokmakov, P., Zakharov, S., and Vondrick, C. Zero-1-to-3: Zero-shot one image to 3d object. In *Proceedings of the IEEE/CVF International Conference on Computer Vision*, pp. 9298–9309, 2023a.

- Liu, Y., Lin, C., Zeng, Z., Long, X., Liu, L., Komura, T., and Wang, W. Syncdreamer: Generating multiview-consistent images from a single-view image. *arXiv preprint arXiv:2309.03453*, 2023b.
- Long, X., Guo, Y.-C., Lin, C., Liu, Y., Dou, Z., Liu, L., Ma, Y., Zhang, S.-H., Habermann, M., Theobalt, C., et al. Wonder3d: Single image to 3d using cross-domain diffusion. *arXiv preprint arXiv:2310.15008*, 2023.
- Lorensen, W. E. and Cline, H. E. Marching cubes: A high resolution 3d surface construction algorithm. *ACM SIG-GRAPH Computer Graphics*, pp. 163–169, 1987.
- Ma, Y., Tsao, D., and Shum, H.-Y. On the principles of parsimony and self-consistency for the emergence of intelligence. *Frontiers of Information Technology & Electronic Engineering*, 23(9):1298–1323, 2022.
- Mildenhall, B., Srinivasan, P. P., Tancik, M., Barron, J. T., Ramamoorthi, R., and Ng, R. Nerf: Representing scenes as neural radiance fields for view synthesis. *Commun. ACM*, 65:99–106, 2020. URL <https://api.semanticscholar.org/CorpusID:213175590>.
- Nichol, A., Dhariwal, P., Ramesh, A., Shyam, P., Mishkin, P., McGrew, B., Sutskever, I., and Chen, M. GLIDE: Towards Photorealistic Image Generation and Editing with Text-Guided Diffusion Models. In *International Conference on Machine Learning*, 2021.
- Poole, B., Jain, A., Barron, J. T., and Mildenhall, B. Dream-Fusion: Text-to-3D using 2D Diffusion. *arXiv preprint arXiv:2209.14988*, 2022.
- Qin, X., Dai, H., Hu, X., Fan, D.-P., Shao, L., and Van Gool, L. Highly accurate dichotomous image segmentation. In *European Conference on Computer Vision*, pp. 38–56. Springer, 2022.
- Radford, A., Kim, J. W., Hallacy, C., Ramesh, A., Goh, G., Agarwal, S., Sastry, G., Askell, A., Mishkin, P., Clark, J., et al. Learning transferable visual models from natural language supervision. In *International conference on machine learning*, pp. 8748–8763. PMLR, 2021.
- Ramesh, A., Dhariwal, P., Nichol, A., Chu, C., and Chen, M. Hierarchical Text-Conditional Image Generation with CLIP Latents. *arXiv preprint arXiv:2204.06125*, 2022.
- Rombach, R., Blattmann, A., Lorenz, D., Esser, P., and Ommer, B. High-Resolution Image Synthesis with Latent Diffusion Models. In *Proceedings of the IEEE/CVF Conference on Computer Vision and Pattern Recognition*, pp. 10684–10695, 2022.
- Saharia, C., Chan, W., Saxena, S., Li, L., Whang, J., Denton, E., Ghasemipour, S. K. S., Ayan, B. K., Mahdavi, S. S., Lopes, R. G., et al. Photorealistic Text-to-Image Diffusion Models with Deep Language Understanding. *arXiv preprint arXiv:2205.11487*, 2022.
- Schuhmann, C., Vencu, R., Beaumont, R., Kaczmarczyk, R., Mullis, C., Katta, A., Coombes, T., Jitsev, J., and Komatsuzaki, A. LAION-400M: Open Dataset of CLIP-Filtered 400 Million Image-Text Pairs. *arXiv preprint arXiv:2111.02114*, 2021.
- Schuhmann, C., Beaumont, R., Vencu, R., Gordon, C., Wightman, R., Cherti, M., Coombes, T., Katta, A., Mullis, C., Wortsman, M., et al. LAION-5B: An open large-scale dataset for training next generation image-text models. *arXiv preprint arXiv:2210.08402*, 2022.
- Shi, R., Chen, H., Zhang, Z., Liu, M., Xu, C., Wei, X., Chen, L., Zeng, C., and Su, H. Zero123++: a single image to consistent multi-view diffusion base model. *arXiv preprint arXiv:2310.15110*, 2023a.
- Shi, Y., Wang, J., Cao, H., Tang, B., Qi, X., Yang, T., Huang, Y., Liu, S., Zhang, L., and Shum, H.-Y. Toss: High-quality text-guided novel view synthesis from a single image. *arXiv preprint arXiv:2310.10644*, 2023b.
- Shi, Y., Wang, P., Ye, J., Long, M., Li, K., and Yang, X. Mvdream: Multi-view diffusion for 3d generation. *arXiv preprint arXiv:2308.16512*, 2023c.
- Song, J., Meng, C., and Ermon, S. Denoising diffusion implicit models. *arXiv preprint arXiv:2010.02502*, 2020.
- Song, Y., Dhariwal, P., Chen, M., and Sutskever, I. Consistency models. *arXiv preprint arXiv:2303.01469*, 2023.
- Tong, S., Dai, X., Wu, Z., Li, M., Yi, B., and Ma, Y. Incremental learning of structured memory via closed-loop transcription. *arXiv preprint arXiv:2202.05411*, 2022.
- Tremblay, J., Meshry, M., Evans, A., Kautz, J., Keller, A., Khamis, S., Müller, T., Loop, C., Morricall, N., Nagano, K., et al. Rtmv: A ray-traced multi-view synthetic dataset for novel view synthesis. *arXiv preprint arXiv:2205.07058*, 2022.
- Wang, H., Du, X., Li, J., Yeh, R. A., and Shakhnarovich, G. Score jacobian chaining: Lifting pretrained 2d diffusion models for 3d generation. In *Proceedings of the IEEE/CVF Conference on Computer Vision and Pattern Recognition*, pp. 12619–12629, 2023a.
- Wang, Z., Bovik, A. C., Sheikh, H. R., and Simoncelli, E. P. Image quality assessment: from error visibility to structural similarity. *IEEE transactions on image processing*, 13(4):600–612, 2004.

Wang, Z., Lu, C., Wang, Y., Bao, F., Li, C., Su, H., and Zhu, J. Prolificdreamer: High-fidelity and diverse text-to-3d generation with variational score distillation. *arXiv preprint arXiv:2305.16213*, 2023b.

Weng, H., Yang, T., Wang, J., Li, Y., Zhang, T., Chen, C., and Zhang, L. Consistent123: Improve consistency for one image to 3d object synthesis. *arXiv preprint arXiv:2310.08092*, 2023.

Zhang, L., Rao, A., and Agrawala, M. Adding Conditional Control to Text-to-Image Diffusion Models. In *IEEE International Conference on Computer Vision*, 2023.

Zhou, Y., Qi, H., Huang, J., and Ma, Y. Neurvps: Neural vanishing point scanning via conic convolution. *Advances in Neural Information Processing Systems*, 32, 2019.

A. More Qualitative Results

A.1. Comparison on consistent multi-view generation.

In Figure 10, we showcase more cases comparing the quality and pose consistency between the generated novel views and ground truth. It is evident that Ctrl123 generates much more pose and appearance consistent views for instances in the training set.

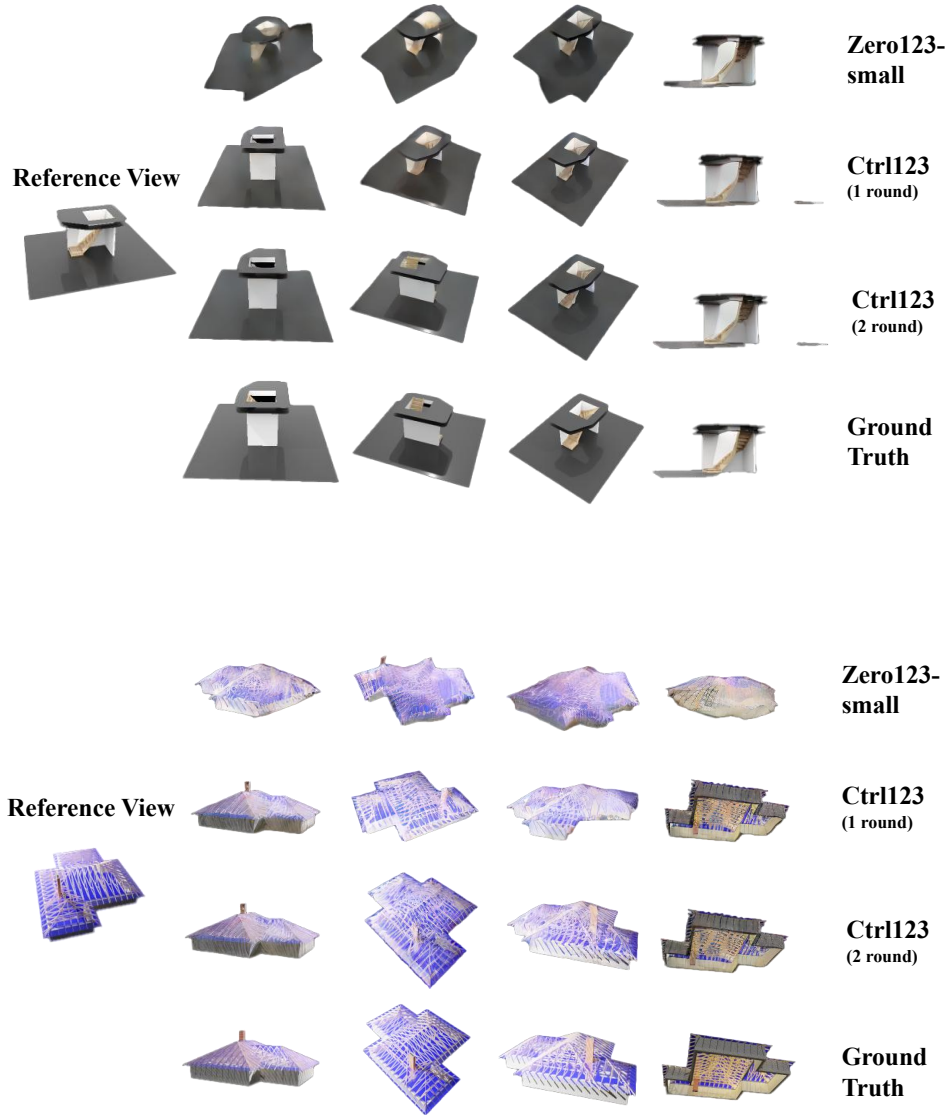


Figure 10. More qualitative comparison of the quality and pose on the generated views with the ground truth views trained on small dataset (25 objects). Comparisons between Zero123-small, Ctrl123, and GT.

A.2. More results generated by Ctrl123 after training on 100K objects.

In this subsection, we present more results of Ctrl123 after large-scale training on Objectverse (Deitke et al., 2023b). In Figure 11, we observe that Ctrl123 generates high-quality novel views on images from the training set; In Figure 12, Ctrl123 also generates high-quality novel views for data outside the training set.

Reference View

Generated Multiview Views

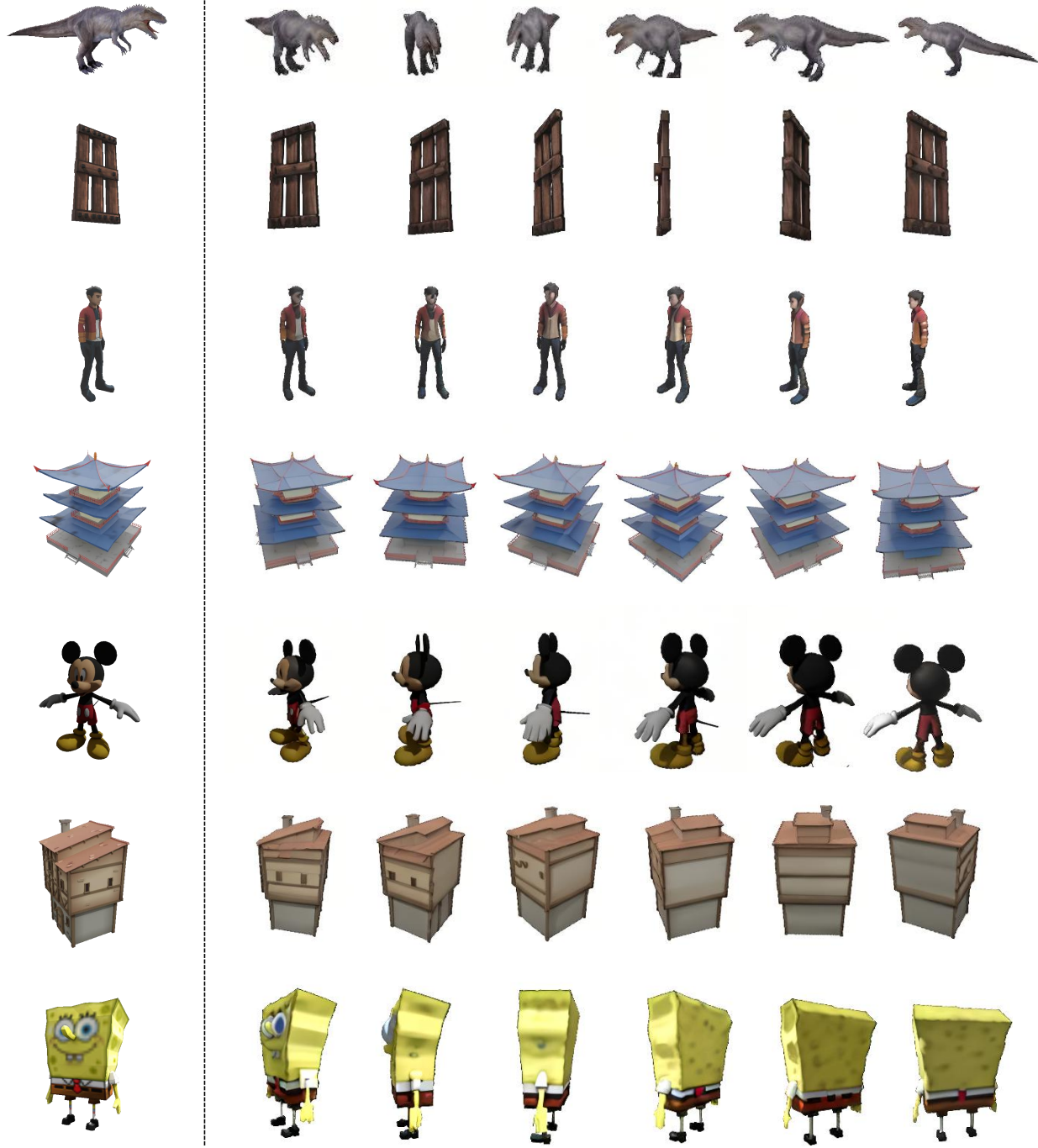


Figure 11. Examples of new views generated by Ctrl123 for images in the training dataset (100K Objaverse (Deitke et al., 2023b)).

Reference View

Generated Multiview Views

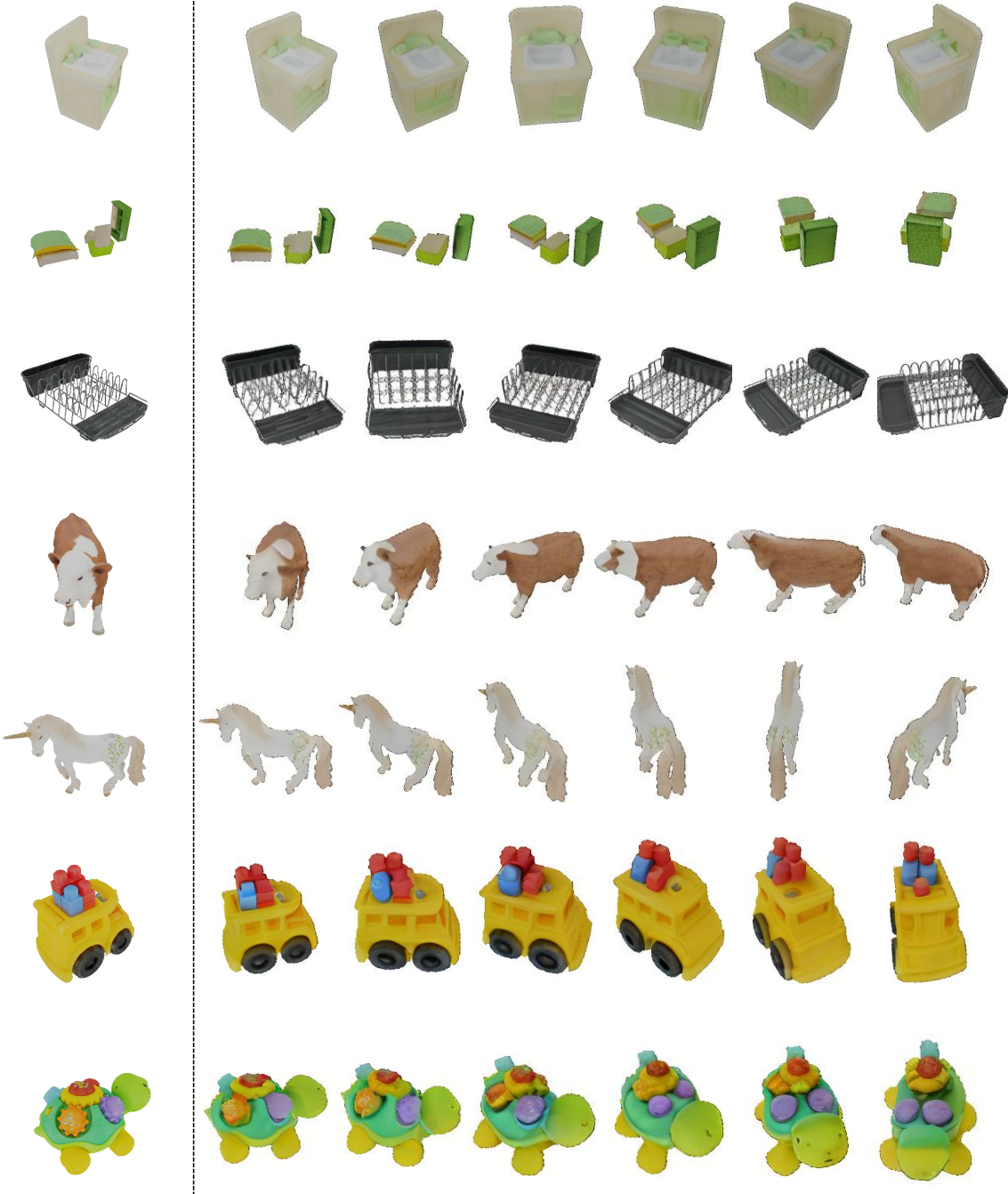


Figure 12. Examples of using Ctrl123 to generate new views for images in the GSO dataset(Downs et al., 2022).

Table 5. Ablation study on different types of consistency losses (pixel space vs latent/feature space).

Consistency Type	Image Quality	Alignment(MegaPose/DIS)
Pixels	KID:0.1490	AA ^{15°} :4.61%
	PSNR:10.6905	IoU ^{0.7} :21.49%
Feature	KID:0.0301	AA ^{15°} :29.75%
	PSNR:18.7103	IoU ^{0.7} :48.19%

Table 6. Comparison of the closed-loop loss on class feature vs patch feature.

Feature Type	Image Quality	Alignment(MegaPose/DIS)
Class Features	KID:0.0677	AA ^{15°} :18.40%
	PSNR:14.5749	IoU ^{0.7} :32.44%
Patch Features	KID:0.0301	AA ^{15°} :29.75%
	PSNR:18.7103	IoU ^{0.7} :48.19%

B. Implementation Details for Image-to-3D Generation

In Section 4.4, we demonstrate the enhancement of 3D reconstruction quality by substituting Zero123 with Ctrl123. All results are obtained using the SDS (Poole et al., 2022) loss implemented by threestudio (Guo et al., 2023). In threestudio, we input one image and train a NeRF(Mildenhall et al., 2020) with 800 training steps. For each training step, we set the noise scale from 0.4 to 0.85. We employ the Adam optimizer(Kingma & Ba, 2014) with $lr = 0.01$, $\beta_1 = 0.9$ and $\beta_2 = 0.99$. After training, in order to get more detailed models, we use marching cube method (Lorensen & Cline, 1987) to export NeRF to mesh.

C. More Ablation Study

Pixel space vs Latent space. To verify the effectiveness of the closed-loop framework, we conducted an ablation study that applies mean square error (MSE) directly between \hat{X}_{tg} and X_{tg} . As shown in Table 5 and Figure 13, enforcing MSE directly in pixel space does not lead to the expected convergence and results in divergence. This highlights the challenges in achieving consistency in different representation spaces.

Closed-loop loss on class features vs patch features. As discussed in section 3.2, the choice of closed-loop loss on the class feature $Z_{tg,c}$ or the patch feature $Z_{tg,p}$ is important for the method. Hence, we conduct the ablation study to experiment with the different choices of class features and patch features. As shown in 6, loss on the patch features could improve the image quality and alignment better than that on the class feature.



Figure 13. Qualitative comparison on the difference type consistency loss (Pixel space vs Latent/feature space).